ELSEVIER

Chemical Engineering Journal 65 (1997) 175–186

Chemical Engineering Journal

Simulation of pH elution in high-performance affinity chromatography using non-porous adsorbents

Jing-Gang Lee, Wen-Chien Lee *, Feng-Sheng Wang

Department of Chemical Engineering, National Chung Cheng University, Chiayi 621, Taiwan

Received 4 March 1996

Abstract

Alteration of the pH of the mobile phase is the most common method to perform elution of the bound components from an affinity column. The values of the adsorption rate constant and the dissociation constant between the protein to be separated from a mixture and the immobilized ligand vary during the chromatographic process. A mathematical model used to predict the performance of pH elution on a high-performance affinity chromatographic column, packed with non-porous adsorbents, has been solved numerically with the application of the finite element method. The effects of binding capacity, sample load, adsorption rate constant and equilibrium dissociation constant under adsorption and elution conditions on the split-peak phenomenon and the shape and spreading of the elution peak were investigated. Simulation results showed that the time required to elute all bound solutes is mainly determined by the dissociation constant which is adjustable by altering the pH of the mobile phase. The dispersive effect on the elution peak is largely influenced by the rate constant under adsorption and elution conditions, while for the non-retained fraction (split-peak), it is governed by the rate and dissociation constants under adsorption conditions only. Influence of sample loading on the non-retained fraction and the elution peak also is significant, especially for columns with small binding capacity. As the affinity column is employed for the purpose of analyzing, a calibration graph based on the height of the elution peak is easily obtained provided that the effects of adsorption rate constant and dissociation constant are all taken into account.

Keywords: Non-porous; Adsorbent; High performance affinity chromatography; pH elution; Split-peak; Peak simulation

1. Introduction

Modeling working on the prediction of chromatographic performance provides an excellent basis for the design and optimization of a liquid chromatographic process operated either in a preparative mode or a high-performance liquid chromatography (HPLC) mode. A great number of papers concerning the simulation of liquid chromatography by the application of numerical methods and computation techniques has been published in the previous decades. In general, the model used to describe the performance of liquid chromatography includes a system of partial differential equations (PDEs) in which the concentrations of solutes in the mobile phase, in the pore (stagnant mobile phase) and on the adsorbent surface (stationary phase) are functions of the axial coordinate of the column, the radial coordinate of the adsorbent radius and the time elapsed. The first step in numerically solving the PDEs system is to discretize the spatial domains (in z and r directions) by one of the following methods: (1) finite difference [1]; (2) orthogonal collocation [2,3]; (3) orthogonal collocation on finite element [4–6]; (4) finite element in the axial combining with orthogonal collocation in the radial direction [7]; (5) orthogonal collocation on finite element in the axial combining with orthogonal collocation in the radial direction [8]. The PDEs system is then transformed into a system of ordinary differential equations (ODEs) with the concentration of solutes at each discretized point as the depending variables of time. The resulting ODEs system, associated with algebraic boundary conditions, is solved by one of the following means: (1) a third-order semi-implicit Runge-Kutta method [3]; (2) a differential/algebraic system solver DASSL [5,6,8], (3) any standard integration routine [2,4], for example, IVPAG in IMSL [1,7]. More computer time is required whenever the elution peaks are much steeper and much greater accuracy of the solution is expected. Early works on simulation of liquid chromatography focused on the solution of frontal analysis, whereas in recent years the trend of research has shifted to zonal elution under isocratic or gradient conditions. Among

* Corresponding author. Fax: +886 52721206; e-mail: chmwcl@ccunix.ccu.edu.tw

1385-8947/97/$17.00
PII S1385-8947(97)00018-1

the great amount of published papers, there have been only a few on the prediction of the chromatographic behaviour (breakthrough curves) of a column packed with non-porous adsorbents [9]. Non-porous adsorbents of small particle diameter have been commonly employed for protein chromatography in recent years. Most non-porous adsorbents are prepared for affinity chromatography of proteins [10–15]. Affinity chromatography operated in the HPLC mode is called high-performance affinity chromatography (HPAC) and has been widely used as an analytical tool in biochemical research. In this work, we focused our attention on the prediction of the elution peaks resulting from pH elution in HPAC.

The model simulation presented in this work also predicates the appearance of 'split-peak' in HPAC. The split-peak phenomena, in which a fraction of solute is eluted at the retention time of a non-retained solute, has been discussed in previous papers [16–20]. Hage et al. [16] obtained an expression that connects the non-retained fraction to the flow-rate, the first-order diffusion rate constant, and a product of the second-order adsorption rate constant and the binding capacity. Including the effect of mass-overload, numerical solutions are also available from computer simulation for the case of irreversible diffusion- and adsorption-limited kinetics [17]. Recently an analytical expression in which the non-retained fraction is related to a non-dimensional lumped adsorption rate constant and the ratio of sample loading to the column capacity, was obtained for irreversible adsorption [18]. This paper describes how the non-retained fraction is influenced by the binding capacity, the sample load, the rate constant and the dissociation constant under various operating conditions.

2. Model description

Consider an affinity column packed with non-porous spherical adsorbents. Assuming that the chromatographic process is isothermal and there is no concentration gradient in the radial direction of the column, the following governing equations for the solute in the mobile phase and on the adsorbent can be obtained.

$$u_0\frac{\partial c}{\partial z}+\epsilon\frac{\partial c}{\partial t}+(1-\epsilon)\frac{\partial q}{\partial t}=\epsilon D_L\frac{\partial^2 c}{\partial z^2} \tag{1}$$

$$\frac{\partial q}{\partial t}=k_a(q_m-q)c_s-k_d q \tag{2}$$

where c_s is the concentration of the solute in the liquid phase at the surface of the particles. As the film mass transfer is considered, the mass balance equation linking the rate of mass transfer in the liquid film and the rate of adsorbate accumulation can be written.

$$(1-\epsilon)\frac{\partial q}{\partial t}=\frac{6(1-\epsilon)k_f}{d_p}(c-c_s) \tag{3}$$

This model is identical to that reported by Mao et al. [9], except for a dispersion term in the right hand side of Eq. (1), which is usually neglected in a typical HPLC system. Only solutions to the breakthrough curve based on this model were reported by Mao et al. [9]. In this work, the chromatogram for a small application of samples to the column, i.e. zonal elution, is our major consideration. The initial and boundary conditions for the chromatography with a rectangular input of sample which has concentration c_0 and injection interval t_{inj} are

$$t=0,\ c=c_s=q=0 \tag{4}$$

and

$$z=0,\ u_0c|_{z=0^-}=u_0c|_{z=0^+}-\epsilon D_L\left.\frac{\partial c}{\partial z}\right|_{z=0^+} \tag{5a}$$

$$\text{with } c|_{z=0^-}=\begin{cases}c_0, & 0\le t\le t_{inj}\\ 0, & \text{otherwise}\end{cases}$$

$$z=L,\ \frac{\partial c}{\partial z}=0 \tag{5b}$$

In Eq. (2), k_a and k_d are respectively the (second-order) adsorption and (first-order) desorption rate constants, which vary with time during the chromatographic process. At the adsorption stage ($t<t_e$), these parameters are determined under the adsorption conditions. After the elution starting at $t=t_e$, these parameters are determined under the elution conditions. In this work, the HPAC of IgG on immobilized protein A as described earlier [21] was taken as the model system for simulation. Samples of human IgG (9 μl) were injected to a column (5×0.46 cm I.D.) packed with non-porous silicas (1.4 μm) covalently coupled with protein A. The elution of the bound proteins was achieved by changing pH of the mobile phase from 7 to 3 at the fifth minute after sample injection. Operating parameters were $\epsilon=0.39$ and $u_0=0.15$ cm/s that corresponded to a flow rate of 1.5 ml/min. To estimate the dispersion coefficients D_L, a correlation developed by Chung and Wen [22] was used.

$$\frac{d_p u_0}{D_L}=0.2+0.011\ \mathrm{Re}^{0.48} \tag{6}$$

where the Reynolds number is defined as $\mathrm{Re}=d_p u_0/\nu$. Based on the parameters of this model system and $\nu=1\times10^{-2}$ cm^2/s (dilute aqueous solution at 293 K), the dispersion coefficient can be calculated using Eq. (6) to be 1.05×10^{-4} cm^2/s. For low Reynolds number, the film-mass-transfer coefficient, k_f, can be estimated from a J factor correlation proposed by Wilson and Geankoplis [23]. This correlation (Eq. (7)) is valid for liquid with a Reynolds number range of 0.0016–55 and a Schmidt number ($\mathrm{Sc}=\nu/D_m$) range of 165–70 600

$$J\equiv\frac{k_f}{u_0}\left(\frac{\nu}{D_m}\right)^{2/3}=\frac{1.09}{\epsilon}\left(\frac{d_p u_0}{\nu}\right)^{-2/3} \tag{7}$$

Taking the experimental value of the molecular diffusivity for human IgG (M.W. 156 000), 4×10^{-7} cm^2/s, k_f can be calculated using Eq. (7) to be 3×10^{-2}cm/s. This k_f value is close to that reported by Mao et al. [9], 3.5×10^{-2} cm/s, for 1.5 μm non-porous particles.

By introducing the following non-dimensional variables: $Z=z/L$, $\tau=u_0t/\epsilon L$, $\mathrm{Pe}=u_0L/\epsilon D_L$, $c^*=c/c_0$, $c_s^*=c_s/c_0$, $q^*=(1-\epsilon)q/\epsilon c_0$, $q_m^*=(1-\epsilon)q/\epsilon c_0$, $k_a^*=k_ac_0L\epsilon/u_0$, $k_d^*=k_d\epsilon L/u_0$ and $k_f^*=6(1-\epsilon)k_fL/d_pu_0$, Eqs. (1)–(3) become

$$\frac{\partial c^*}{\partial Z}+\frac{\partial c^*}{\partial \tau}+\frac{\partial q^*}{\partial \tau}=\frac{1}{\mathrm{Pe}}\frac{\partial^2 c^*}{\partial Z^2} \tag{8}$$

$$\frac{\partial q^*}{\partial \tau}=k_a^*(q_m^*-q^*)c_s^*-k_d^*q^* \tag{9}$$

and

$$\frac{\partial q^*}{\partial \tau}=k_f^*(c^*-c_s^*) \tag{10}$$

Based on the above-mentioned values of D_L and k_f, the non-dimensional mass transfer coefficients are $\mathrm{Pe}=18\,300$ and $k_f^*=26\,100$. Even when the flow velocity is reduced from 0.15 to 0.05 cm/s, the figures of the non-dimensional mass-transfer parameters are still at the same level. These extremely higher values of mass transfer coefficients indicate that the mass transfer resistance raised by both axial dispersion and liquid film can be neglected. In this instance, Eq. (10) can be eliminated from the governing equations and c_s^* can be approximated by c^* for any time. Eq. (9) can thus be replaced by

$$\frac{\partial q^*}{\partial \tau}=k_a^*(q_m^*-q^*)c^*-k_d^*q^* \tag{11}$$

It is noted that $k_a^*/k_d^*=k_ac_0/k_d=c_0/K_d$, where K_d is the equilibrium dissociation constant for the solute and immobilized ligand. The rate constants, k_a and k_d, are determined by the chosen affinity pair and subject to evaluation from experiments, whereas K_d or its reciprocal K_a (equilibrium association constant) is a thermodynamic variable that can be adjusted by changing the mobile phase pH and/or ionic strength. A higher value of Peclet number indicates that the effect of axial dispersion is insignificant. However, we keep this dispersion term in Eq. (8) for the sake for numerical implementation. The non-dimensional forms of initial and boundary conditions for solving Eqs. (8) and (11) are

$$\tau=0,\ c^*=q^*=0 \tag{12}$$

$$Z=0,\ \left.\frac{\partial c^*}{\partial Z}\right|_{Z=0^+}=\mathrm{Pe}(c^*|_{Z=0^+}-c^*|_{Z=0^-})$$

$$\text{with } c^*|_{Z=0^-}=\begin{cases}1, & 0\le\tau\le u_0t_{inj}/\epsilon L\\ 0, & \text{otherwise}\end{cases} \tag{13a}$$

$$Z=1,\ \frac{\partial c^*}{\partial Z}=0 \tag{13b}$$

An analytical solution is available only when the kinetic constants are at a constant value, i.e. chromatography in the mode of isocratic elution. In this instance, Goldstein [24] obtained a closed form solution to zonal elution with an infinite value of Pe. For a typical operation in affinity chromatography, the pH of the elution buffer differs from that of adsorption buffer, which means that values of the kinetic constants vary during the chromatographic process. Numerical method must be employed for the simulation and prediction of the performance of the elution peaks.

3. Numerical method

Eqs. (8) and (11) were discretized into a set of ordinary differential equations (ODEs) by the Galerkin finite element method using quadratic shape functions as the trial (basis) functions. According to this numerical method, first we broke the domain $0\le Z\le1$ into $n-1$ elements with a size of ΔZ $(=1/(n-1))$ using n nodes. The approximate solutions for c^* and q^* thus could be expressed as the linear combinations of the trial functions:

$$c^*=\sum_{i=1}^{n}c_i(\tau)g_i(Z) \tag{14}$$

$$q^*=\sum_{i=1}^{n}q_i(\tau)g_i(Z) \tag{15}$$

where each trial function g_i is defined only on the appropriate elements [25,26]. According to the Galerkin method, the residuals are formed by substituting the trial functions into Eqs. (8) and (11) with c^* and q^* approximated by Eqs. (14) and (15) [25]. The residuals at the nodes are

$$\begin{aligned}\sum_{i=1}^{n}\dot{c}_i\int_0^1 g_ig_j\mathrm{d}Z=&-\sum_{i=1}^{n}c_i\int_0^1 g_{Z_i}g_j\mathrm{d}Z\\&+(\mathrm{Pe}^{-1})\sum_{i=1}^{n}c_i\int_0^1 g_{ZZ_i}g_j\mathrm{d}Z+k_a^*q_m^*\sum_{i=1}^{n}c_i\int_0^1 g_ig_j\mathrm{d}Z\\&+k_d^*\sum_{i=1}^{n}q_i\int_0^1 g_ig_j\mathrm{d}Z+k_a^*\int_0^1\sum_{i=1}^{n}q_ig_i\sum_{k=1}^{n}c_k\int_0^1 g_kg_j\mathrm{d}Z\end{aligned} \tag{16}$$

$$\begin{aligned}\sum_{i=1}^{n}\dot{q}_i\int_0^1 g_ig_j\mathrm{d}Z=&k_a^*q_m^*\sum_{i=1}^{n}c_i\int_0^1 g_ig_j\mathrm{d}Z\\&+k_d^*\sum_{i=1}^{n}q_i\int_0^1 g_ig_j\mathrm{d}Z+k_a^*\int_0^1\sum_{i=1}^{n}q_ig_i\sum_{k=1}^{n}c_k\int_0^1 g_kg_j\mathrm{d}Z\end{aligned} \tag{17}$$

for $j=1,2,\ldots n$. In Eqs. (16) and (17), the definite integrals of the trial functions and their derivatives with respect to coordinate variable Z can easily be estimated according to a typical book of numerical method [25]. A system of $2n$ ODEs

is then constructed with c_i and q_i as the functions of τ and $\dot{c}_j$ and $\dot{q}_j$ as the time derivatives of these variables. However, the concentrations at two ends of the column, c_1 and c_n, can be eliminated from Eqs. (16) and (17) by the application of boundary conditions, Eq. (13a) and (13b), as suggested by Lipidus and Pinder [26]. Substituting Eqs. (14) and (15) into Eq. (13a) and (13b) yields

$$c_1 = \left[c|_{Z=0^-} + \frac{2(1/\mathrm{Pe})}{\Delta Z} c_2 - \frac{1/\mathrm{Pe}}{2\Delta Z} c_3 \right] \Big/ \left[1 + \frac{2(1/\mathrm{Pe})}{2\Delta Z} \right] \quad (18)$$

$$c_n = \frac{-1}{3} c_{n-2} + \frac{4}{3} c_{n-1} \quad (19)$$

The number of ODEs becomes $2n-2$. This system of ODEs was solved using Gear's stiff method by calling a subroutine IVPAG in IMSL.

4. Results and discussion

4.1. Convergence of numerical solutions

The parameters used in model simulation for the results presented by the figures in this paper are listed in Table 1. To test the validity of the simulated solutions, peak profiles under limiting conditions were considered. Fig. 1 shows two chromatographic peaks respectively for columns with small ($q_m = 1$ g/l) and large binding capacity ($q_m = 35$ g/l), operated in the mode of isocratic elution as a typically weak affinity column does. As expected, the agreement between numerical solutions (solid lines) and Goldstein solutions (circle points) is quite good. The elution time is shorter whenever the binding capacity is lower; this is because the retention time is proportional to binding capacity. Under the conditions of linear chromatography, the mean retention time can be predicted by the following equation

$$t_R = \frac{t_{inj}}{2} + \frac{\epsilon L}{u_0}(1 + k_0') \quad (20)$$

where $k_0 = (1-\epsilon) q_m / (\epsilon K_d)$ is the limiting capacity factor, i.e. the capacity factor at zero sample concentration. From Fig. 1, it can be seen that the elution peak is sharper when q_m is small and the peak becomes broader and lower when q_m is large. At a limiting case when an infinitesimal sample load is applied to the column, the central second moment of the elution peak is linearly proportional to a ratio of the binding capacity to the desorption rate constant. The second central moment stands for the square of the peak width. Numerical solutions can induce an oscillation with an insignificant magnitude far from the tail side of the peak as shown in Fig. 1(b). The oscillation, however, will not affect the convergence of the peak height and area of the elution.

Influences of the element number on the convergence of the simulated peaks are shown in Fig. 2. If the axial domain is separated by n nodes, there are $N_e = (n-1)/2$ elements. It is observed that occasionally there are oscillations around the first peak (i.e. the non-retained peak) whenever N_e is smaller. Those oscillations will disappear when N_e is equal to or greater than 100, i.e. $n \geq 201$. On the contrary, no oscillation

Table 1
Parameters used in model simulation

Fig. No.	Curve No.	k_a, adsorption ($1\,g^{-1}\,s^{-1}$)	K_d, adsorption (M)	k_a, elution ($1\,g^{-1}\,s^{-1}$)	K_d, elution (M)	C_0 (g/l)	q_m (g/l)
1	a	0.7	1.282×10^{-5}	0.7	1.282×10^{-5}	10	1
	b	0.7	1.282×10^{-5}	0.7	1.282×10^{-5}	10	35
2		0.0075	10^{-8}	0.75	1.282×10^{-5}	10	35
3, 5		0.01–0.3	10^{-8}	0.7	1.282×10^{-5}	10	35
4, 6		0.3–0.8	10^{-9}	5	2×10^{-7}	10	1
7		0.1	10^{-9}–10^{-6}	0.7	1.282×10^{-7}	10	35
8, 9		0.1	10^{-9}–10^{-6}	0.7	2×10^{-7}	10	1
10	1	0.2625	0	5	1.282×10^{-5}	0–40	1
	2	0.0262					10
	3	0.0075					35
11		0.1	10^{-8}	0.1–2.5	1.282×10^{-5}	10	35
12		0.1	10^{-8}	0.7	7.5×10^{-6}–1×10^{-4}	10	35
13	1	0.1	10^{-8}	0.7	1.282×10^{-5}	10	35
	2				7.325×10^{-6}		20
	3				3.66×10^{-6}		10
	4				3.66×10^{-7}		1
14		0.4	10^{-9}	5	2×10^{-7}	10–30	1
15		0.0075	10^{-6}–10^{-8}	3	1.282×10^{-5}	0–40	35
16, 17	1	0.75	2.15×10^{-9}	5	2.15×10^{-7}	10	1
	2	0.45	2.15×10^{-9}	5	2.15×10^{-7}	20	1

Other parameters not listed are: $\epsilon = 0.39$, $u_0 = 0.15$ cm/s, $L = 5$ cm, $P_e = 18\,300$, and the sample volume is 9 μl, which corresponds to $u_0 t_{inj}/\epsilon L = 9/320$. Elution begins at the fifth minute from the injection of the sample. The molecular weight of the solute (human IgG) is 156 000, so that a K_d value of 1.282×10^{-5} M corresponds to 2 g/l.

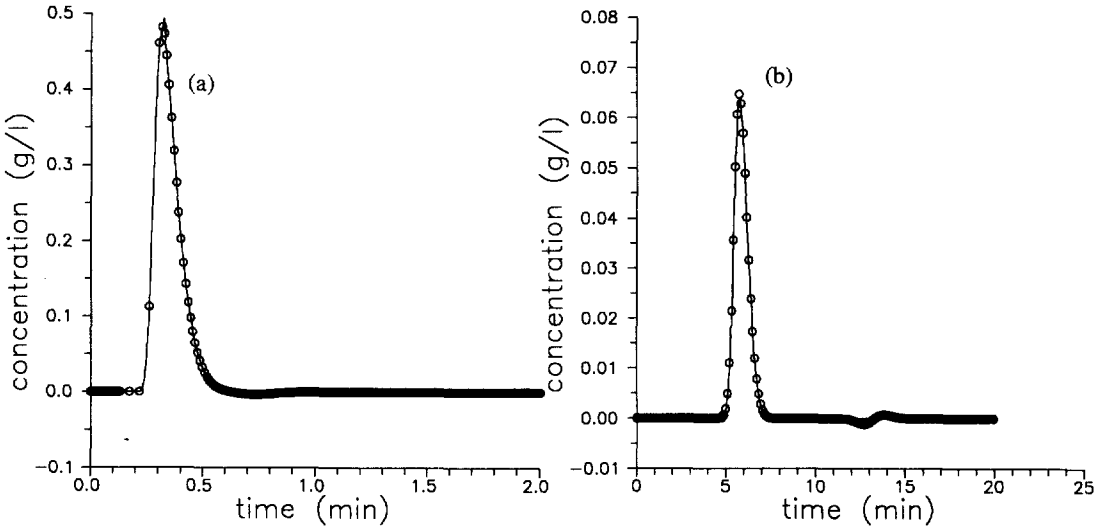

Fig. 1. Comparison of isocratic elution profiles from model simulations (solid lines) and Goldstein solutions (circle points) with different binding capacity, q_m (g/l): (a) 1; (b) 35.

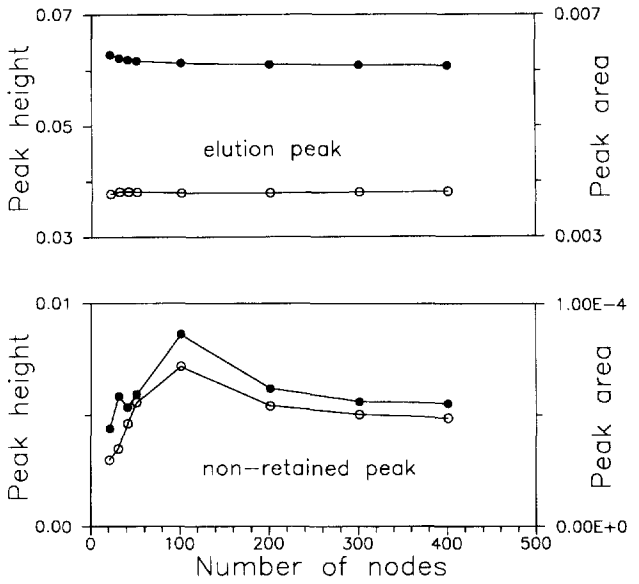

Fig. 2. Dependence of the peak height (○) and peak area (●) on the number of nodes for the discretization of the axial coordinate in the application of the finite element method.

is observed around the second peak (the elution peak). When $n = 101$, the height and area of the second peak are observed to be converging to the exact values. On the other hand, it requires 301 or more nodes for the convergence of the peak height and peak area of the first peak. It is concluded that the number of nodes that is required for convergence is determined by the steepness of the peak front, which is dependent on the rate parameters. The non-retained peak is always small in area and steeply peaked. If the chromatographic system does not have a non-retained peak, a small number of nodes will be enough for numerical computation to yield accurate solutions.

4.2. *Effects of dissociation and kinetic rate constants at the adsorption stage*

In this simulation, the model system involves a strong affinity interaction between the protein in the mobile phase and the immobilized ligand with a K_d value of 10^{-8} M under the adsorption conditions. The peak profiles with various k_a (adsorption) values ranging from 0.01 to 0.3 l g^{-1} s^{-1} are given in Fig. 3. As the K_d and k_a at the elution stage are respectively kept constant at 2 g/l ($= 1.282 \times 10^{-5}$ M) and 0.71 g^{-1} s^{-1}, the non-retained peak appears only when k_a (adsorption) $= 0.01$ l g^{-1} s^{-1}. Fig. 4 shows peak behaviour of a small capacity system with $K_d = 10^{-9}$ M at the adsorption

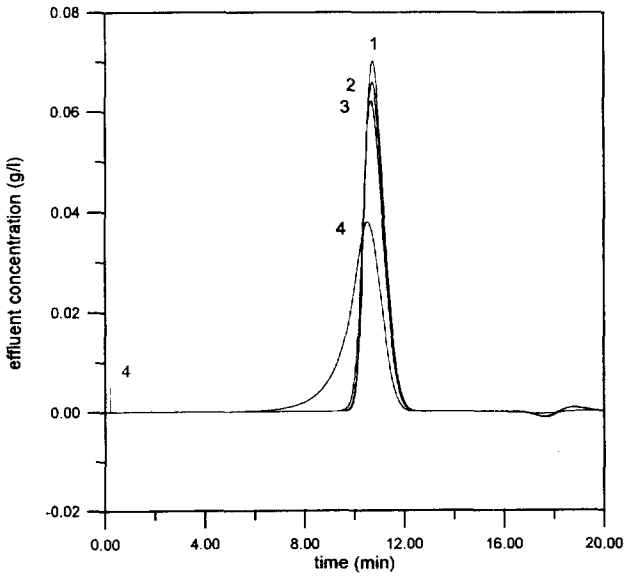

Fig. 3. Elution profiles simulated with a larger binding capacity ($q_m = 35$ g/l) and a different adsorption rate constant, k_a (l g^{-1} s^{-1}), at the adsorption stage: (1) 0.3; (2) 0.1; (3) 0.05; (4) 0.01. The split-peak appears in curve 4.

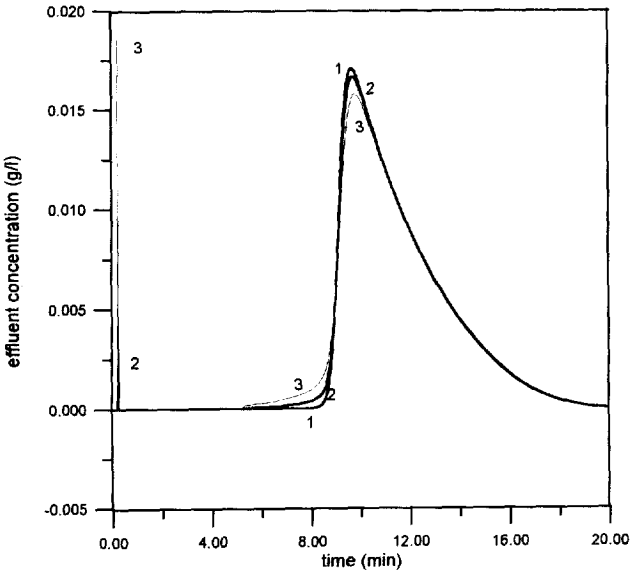

Fig. 4. Elution profiles simulated with a smaller binding capacity ($q_m = 1$ g/l) and a different adsorption rate constant, k_a (l g^{-1} s^{-1}), at the adsorption stage: (1) 0.8; (2) 0.4; (3) 0.3. The split-peak appears in both curves 2 and 3.

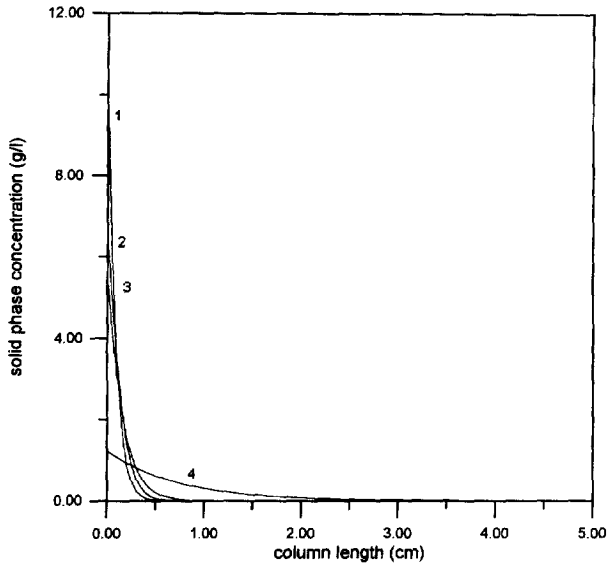

Fig. 5. Distributions of the adsorbate concentration at the starting time of the elution stage as functions of the axial distance along the column for the chromatographic systems corresponding to Figs. 5 and 3.

stage and $K_d = 2 \times 10^{-7}$ M and $k_a = 5$ l g^{-1} s^{-1} at the elution stage. There is a non-retained peak when k_a (adsorption) is reduced to 0.4 l g^{-1} s^{-1}. A small value of k_a stands for a slow adsorption rate. For a column with small binding capacity, the critical k_a value required for the appearance of the non-retained peak is higher. Fig. 6 show the profiles of adsorbate as functions of the abscissa along the column at the time when the elution starts, i.e. the q–z plots at the fifth minute after sample injection. Fig. 5 indicates that only a small portion of the adsorbents near the column entrance are bound with the solutes in the system with larger binding capacity. But for a column with small binding capacity, the distribution of the adsorbate concentration covers a wider range of the axial distance along the column as shown in Fig. 6. The profile of the adsorbate concentration is more dispersed and the binding sites of the adsorbents including the end of the column are occupied by the solutes (curve 3 in Fig. 6). Figs. 3–6 show that an increase in k_a (adsorption) sharpens the elution peak and elevates the adsorbate concentration at the entrance region of the column. A lower value of k_a occasionally results in a non-retained peak. In summary, for a column with small binding capacity the elution peaks are much lower and dispersed, and are right triangle shaped. Whereas for a column with large binding capacity, only the adsorbents near the column entrance are bound with the solutes and the elution peaks are taller and sharply shaped.

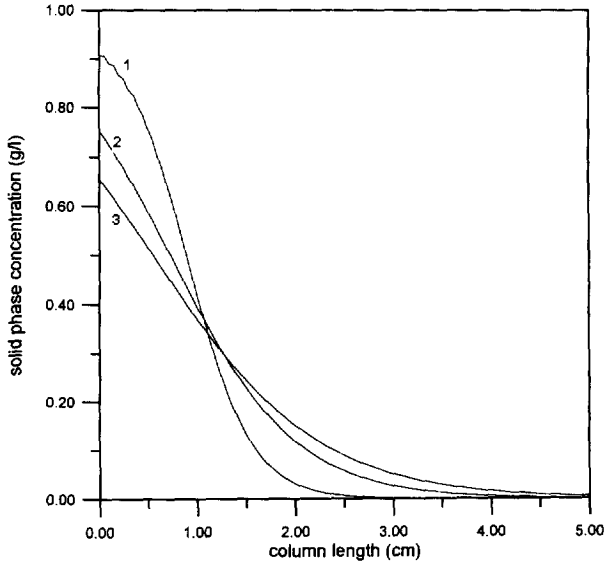

Fig. 6. Distributions of the adsorbate concentration at the starting time of the elution stage as functions of the axial distance along the column for the chromatographic systems corresponding to Fig. 4.

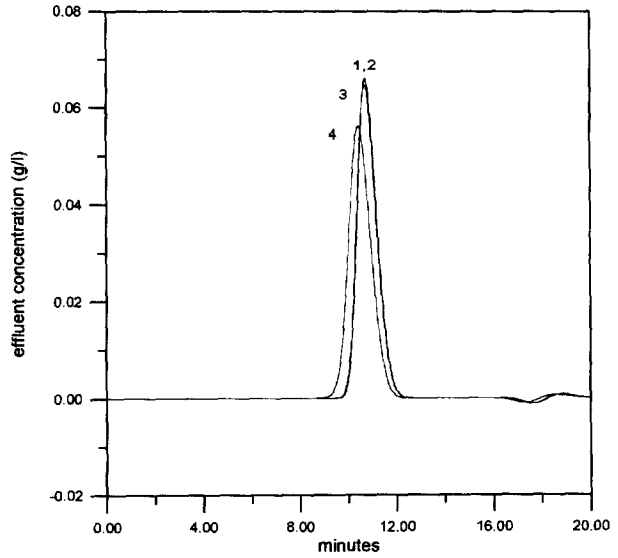

Fig. 7. Elution profiles simulated with a larger binding capacity ($q_m = 35$ g/l) and a different equilibrium dissociation constant, K_d (M), at the adsorption stage: (1) 10^{-9}; (2) 10^{-8}; (3) 10^{-7}; (4) 10^{-6}.

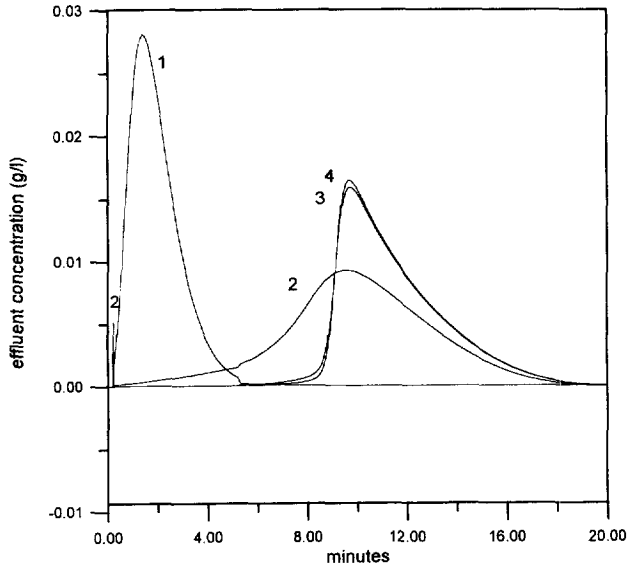

Fig. 8. Elution profiles simulated with a smaller binding capacity ($q_m = 1$ g/l) and a different equilibrium dissociation constant, K_d (M), at the adsorption stage: (1) 10^{-6}; (2) 10^{-7}; (3) 10^{-8}; (4) 10^{-9}. The split-peak appears in curve 2.

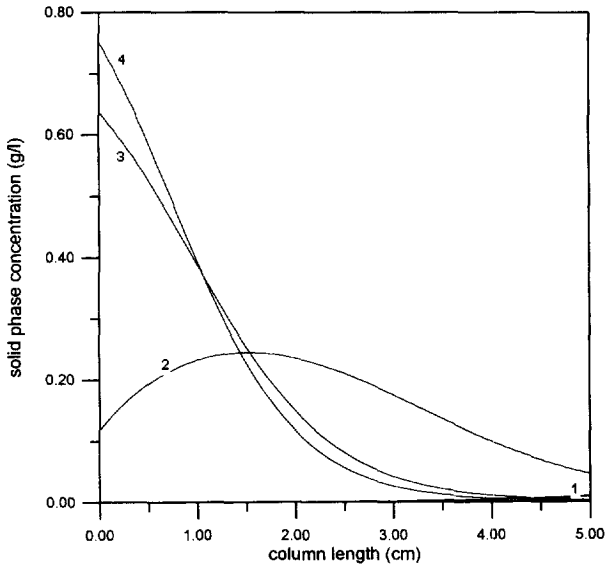

Fig. 9. Distributions of the adsorbate concentration at the starting time of the elution stage as functions of the axial distance along the column for the chromatographic systems corresponding to Fig. 8.

Effects of dissociation constant (ranging from 10^{-9} to 10^{-6} M) at the adsorption conditions on the peak profiles is shown in Figs. 7 and 8 respectively for high and low ligand density columns. These figures show that when K_d increases, the elution peak becomes more dispersed and slightly advanced. As K_d falls in the range of 10^{-8}–10^{-9} M (approaches to the irreversible adsorption), the peak behaviour is nearly unaltered. In the system with small binding capacity, most of the ligates are eluted together as the non-retained component (Fig. 8) when K_d increases to a value of 10^{-6} M. A medium value of K_d (10^{-7} M) results in a small fraction of non-retained component and the q–z distribution is more even than the others (Fig. 9).

4.3. Non-retained fraction

The 'split-peak' phenomenon occurs with low enough adsorption rate constant or large enough mobile-phase velocity, either in linear or mass-overloading conditions. The definition for the intensity of the split-peak effect (non-retained fraction), which is characterized by the ratio of the amount eluted in the first peak (the non-retained peak) to the injected amount, is given by

$$f = \frac{\int_{\text{first peak}} c(t, z=L)\,dt}{c_0 t_{inj}} \tag{21}$$

wherein f depends on k_a and K_d at the adsorption conditions. For constant values of q_m and K_d, Fig. 4 shows that the non-retained peak comes whenever k_a is small enough. For constant values of q_m and k_a, an increase in K_d increases the value of f (Fig. 8). Both Figs. 4 and 8 are simulated results from a column with binding capacity $q_m = 1$ g/l and sample concentration $c_0 = 10$ g/l. According to the literature, the non-retained fraction under irreversible adsorption can be estimated by the following expression [18]

$$f = \frac{\ln[1 + (e^{NQ_i/Q_x} - 1)e^{-N}]}{NQ_i/Q_x} \tag{22}$$

where Q_i/Q_x is a loading factor, which is equal to the ratio of the amount of solute injected to the column ($Q_i = u_0 A_c c_0 t_{inj}$) to the stationary capacity of the column ($Q_x = (1-\epsilon)A_c L q_m$). It can be proved that this loading factor standing for the relative sample loading with respect to the binding capacity of the column is identical to z_0/L. The parameter N ($= k_a(1-\epsilon)q_m L/u_0$) in Eq. (22) is a product of the non-dimensional adsorption rate constant and the binding capacity. The dependence of f on the sample concentration (in 9 μl) for various values of q_m under irreversible adsorption is illustrated in Fig. 10. It can be seen that the simulated results closely approximate those predicted by Eq. (22). The validity of the simulate results from the computational algorithm employing the finite element method are thus confirmed again. The non-retained fraction is significantly affected by the increase in sample loading for a column with smaller q_m (lower ligand density), but f is insignificantly altered by the loading of sample for a column with larger q_m (higher ligand density).

In summary, it is observed that the non-retained fraction is governed by k_a and K_d under the adsorption conditions as well as by the sample loading. The non-retained fraction increases with the decrease of k_a and/or K_d. Besides being able to predict the occurrence of the split-peak effect under irreversible adsorption as Eq. (22), the model simulation is also applicable to a case in which there is a finite dissociation constant.

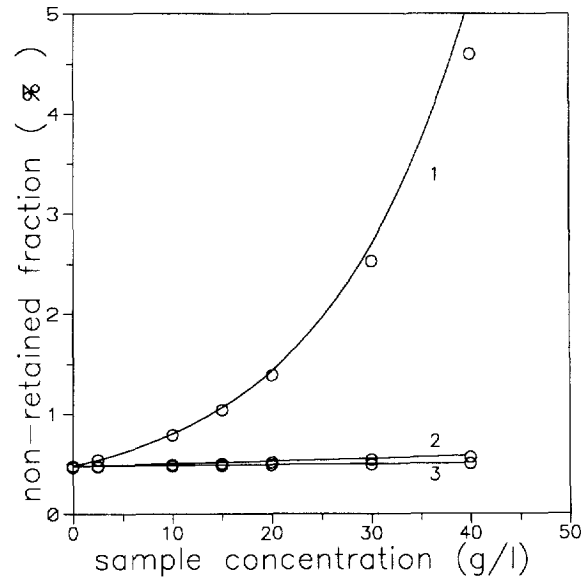

Fig. 10. Non-retained fraction as a function of sample load under the conditions of irreversible adsorption with different adsorption rate constant, k_a ($l\ g^{-1}\ s^{-1}$), at the elution stage: (1) 0.2625; (2) 0.0262; (3) 0.0075. Results from model simulation (circle points) are comparable to the values calculated (solid curves) by Eq. (22).

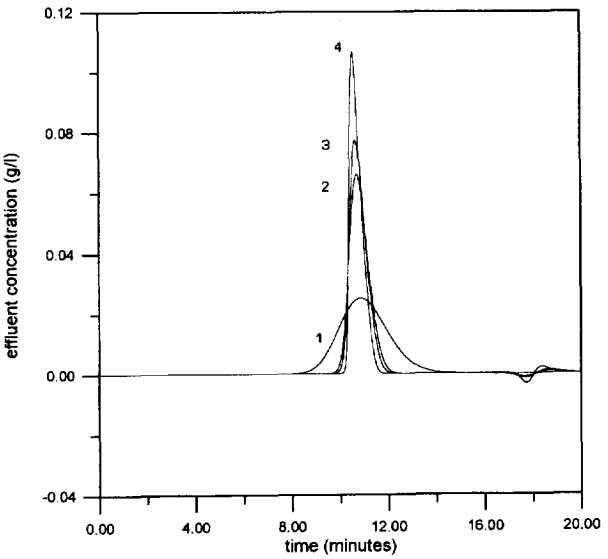

Fig. 11. Elution profiles simulated with different adsorption rate constant, k_a ($l\ g^{-1}\ s^{-1}$), at the elution stage: (1) 0.1; (2) 0.7; (3) 1.0; (4) 2.5.

4.4. *Effects of dissociation and kinetic rate constants at the elution stage*

When the dissociation constant remains unchanged, the larger k_a value corresponds to the larger k_d value. The large values of k_d and k_a under elution conditions indicate a rapid desorption rate of the bound compounds from the adsorbent and a rapid re-adsorption rate of the unbound compounds to the adsorbent. Fig. 11 shows that when the rate constants become larger, the elution peak becomes sharper and the time required to elute all bound solutes becomes shorter due to the faster rate. The peak height increases with the rate constant owing to the sharper peak and constant value of the peak area. The rate constant may possibly be difficult to adjust as it is largely determined by the chosen protein–ligand system and slightly dependent on mobile phase composition and pH.

The elution of the bound proteins (solutes) from adsorbent in affinity chromatography is typically achieved by increasing the dissociation constant in the mobile phase under the elution conditions. A larger K_d implies a weak binding affinity between the protein and the immobilized ligand. Decreasing K_d significantly delays the appearance of the elution peak, as shown in Fig. 12. It can be seen from Fig. 12 that the mean retention time of the eluted peak and the time required to conclude the elution become shorter due to weaker binding. The equilibrium dissociation constant is a thermodynamic property and is dependent on the pH, ionic strength and the composition of the mobile phase at the elution stage. Alteration of the pH of the mobile phase is one of the most common ways of increasing the K_d value. However, it is generally impractical to increase K_d by altering pH to an extremely low or high value. The strong elution conditions under the extreme pH values that result in a higher K_d value usually lead to serious damage to the product and ligand. This is especially true for the protein ligand which may be irreversibly damaged by a strong elution in immunoaffinity chromatography.

For an analytical propose, the elution time should be as short as possible. Eq. (20) indicates that a small ratio of q_m to K_d gives a faster elution. Fig. 13 shows elution peaks for various combinations of q_m and K_d, in which the ratio q_m/K_d is made to be 17.5. It can be seen that a higher q_m and lower K_d corresponds to a sharper peak. Decreases in q_m and increases in K_d result in slightly shorter retention times owing to the effect of mass overloading and a much dispersed elution peak. There exits a non-retained peak as q_m is reduced to unity. It is concluded that if K_d can not be extensively promoted, a lower ligand density should be considered as an alternative. The ligand density (binding capacity) can be adjustable through the control of the conditions of ligand

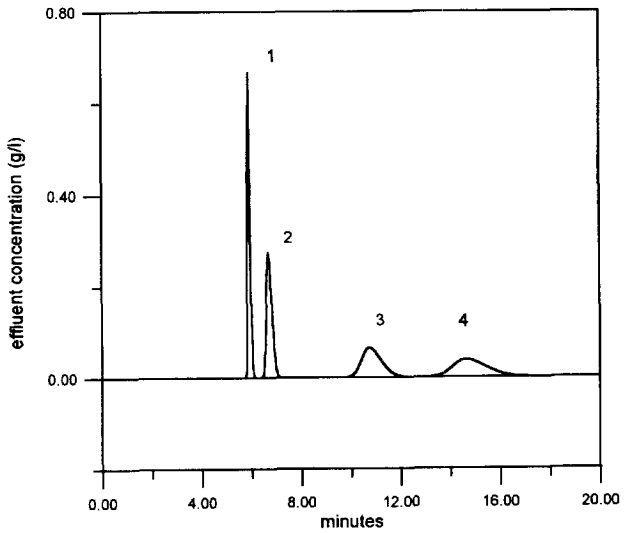

Fig. 12. Elution profiles simulated with different equilibrium dissociation constant, K_d (M), at the elution stage: (1) 10^{-4}; (2) 4.75×10^{-5}; (3) 1.282×10^{-5}; (4) 7.5×10^{-6}.

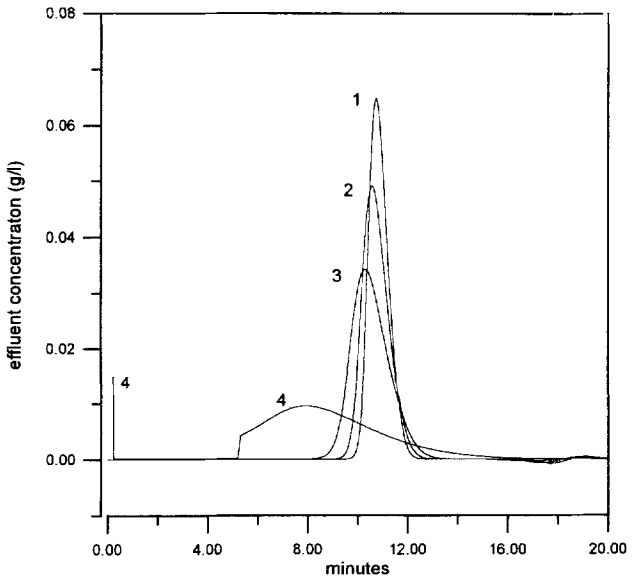

Fig. 13. Elution profiles simulated with different combination of q_m and K_d. The value of q_m/K_d is kept at 17.5, whereas q_m is: (1) 35; (2) 20; (3) 10; (4) 1. The split-peak appears in curve 4.

immobilization. There is still much flexibility in this adjustment for the use of non-porous adsorbents as the stationary phase which posseses small surface area. Experimental results from the adsorption of lysozyme on silica-based affinity adsorbents indicate that the binding capacity of the non-porous adsorbent is comparable to that of porous adsorbent [12].

As the adsorbents are made and the column packed, the binding capacity, the rate constant and the dissociation constant can be evaluated, separately or simultaneously, in a sequence of batch or frontal experiments. The dependence of pH on the variation of K_d is easily obtained experimentally [27,28]. As the binding capacity and the rate constant are determined and the relationship between pH and dissociation constant is known, the elution peaks can be predicted by the model simulation. The peaks generated from the model simulation can be used to obtain performance information of pH elution necessary to design the analytical process, such as the non-retained fraction, the band broadening, and the time required to conclude the analysis under various operating conditions.

4.5. *Effects of sample loading*

Modeling Eqs. (8)–(11) indicates that the peak profiles are determined by the parameters ϵ, u_0, L, t_{inj}, c_0, q_m, k_a and K_d, when the contribution of Pe and k_f^* is negligible. If the affinity column is made by following a constant procedure and operated under analytical conditions as a typical HPLC column, influences of ϵ, u_0, L and t_{inj}, on the peak behaviour can be easily calculated. An increase in flow velocity, for example, causing a reduction in the elution time is obvious from the definition of the non-dimensional time $\tau = tu_0/\epsilon L$. The sample concentration, in addition to the binding capacity and the kinetic constants, is the most important factor influencing the elution profiles. Variation of elution peak with concentration of sample (9 μl) injected to the column is given in Fig. 14. Both the area and height of the first and second peaks from simulation increase with increasing sample load. The elution peak becomes sharper in the front side at heavy sample loading. The shape of the elution profile turns from a symmetric and dispersed peak to shaped as a right triangle and as an asymmetric triangle as c_0 increases.

When the HPAC column is operated for an analytical purpose, the calibration graph based on peak height will be much simpler than that on the peak area. Although the height of the elution peak definitely increases with sample load, this dependence is influenced by the rate constants. Fig. 15 shows that straight lines passing through the origin can be obtained from the plots of peak height vs. sample load for larger values of K_d, based on a constant value of k_a. The loci of the peak height become slightly curvilinear over the range of sample load as K_d (adsorption) decrease to 10^{-7} and 10^{-8} M. For slow adsorption system with K_d from 10^{-6} to 10^{-8} under adsorption conditions, a small K_d corresponds to a small desorption rate constant k_d if k_a is kept constant. The adsor-

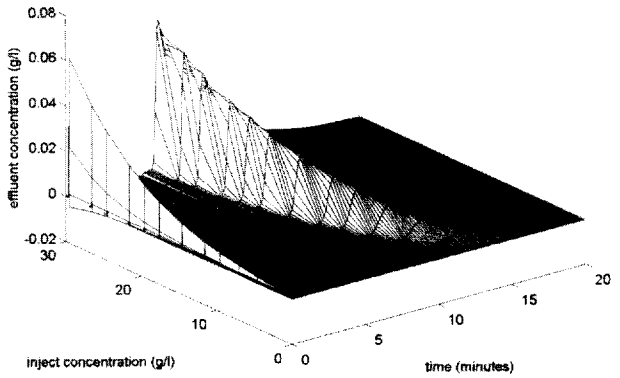

Fig. 14. Elution profiles simulated with various sample concentrations ranging from 10–30 g/l.

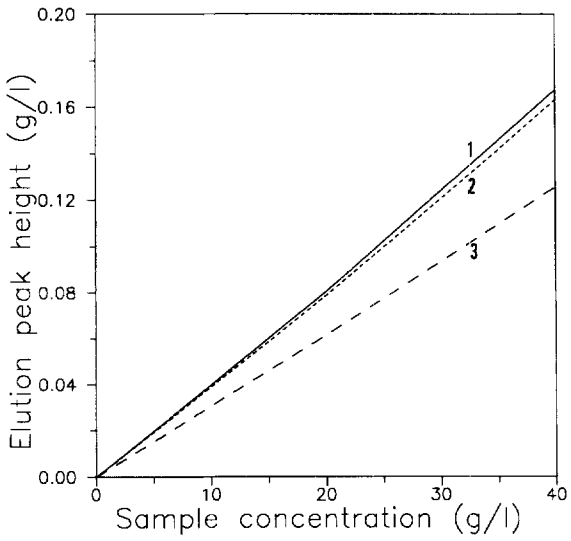

Fig. 15. Plots of peak height solute concentration in 9 μl samples for several values of K_d (M) at the adsorption stage: (1) 10^{-8}; (2) 10^{-7}; (3) 10^{-6}.

bates are more concentrated in the entrance region of the column and the elution peak is more dispersed with a lower peak height as shown in Fig. 7 when K_d becomes smaller. In summary, other plots such as Fig. 15 can be obtained based on the variation of other kinetic parameters: k_a (adsorption), k_a (elution) or K_d (elution). In general, an increase in k_a or K_d, either at the adsorption or elution stage, results in an increase in the height of the elution peak. The calibration graph should be carefully drawn in any instance.

4.6. Elution followed an irreversible adsorption

When the adsorption is irreversible (i.e. $K_d = 0$ at adsorption stage), the column becomes saturated with adsorbates from the entrance end. At the starting time of the elution, the q–z profile is $q = q_m$ for $1 < z \le z_0$ and $q = 0$ for $z_0 < z \le L$. The ratio z_0/L is the relative sample load with respect to the total binding capacity of the column. The distribution describing the elution peak can be written as Eq. (23), provided that the axial dispersion effect is negligible [21].

$$c(\tau, z=L) = K_d\sqrt{k_0'/(\tau-1)} \times \frac{I_1(2k_d^*\sqrt{k_0'(\tau-1)})[1-e^{-k_0'k_d^*z_0/L}]}{I_0(2k_d^*\sqrt{k_0'(\tau-1)}) + \Phi[k_d^*(\tau-1), k_0'k_d^*] + e^{-k_0'k_d^*z_0/L}\Phi[k_0'k_d^*, k_d^*(\tau-1)]} \quad (23)$$

Φ stands here for the function

$$\Phi(u,v) = e^u \int_0^u e^{-s} I_0(2\sqrt{vs})\,ds \quad (24)$$

In Eqs. (23) and (24), I_0 and I_1 are respectively the modified Bissel functions of zeroth and first order. For irreversible adsorption, Eq. (23) describes simply the dependence of the elution profiles on the loading factor defined by z_0/L and two additional parameters, K_d (elutions) and k_d^* (or in terms of k_a^*). Fig. 16 shows two q–z profiles at the fifth minute after sample injection for a column with a strong affinity interaction ($K_d = 2.15 \times 10^{-9}$ M at adsorption stage). These q–z profiles are not exactly of the rectangular type as that for irreversible adsorption though the K_d value is extremely small. If these q–z profiles are approximated by rectangular profiles as presented by the dashed curves in Fig. 16, the simulated elution peaks (the second peaks) as shown in Fig. 17 agree well with those predicted by Eq. (23) using the approximated q–z profiles. This approximation is valid even in a case in which there is a small amount of non-retained fraction (curve 2 in Fig. 17). It can be concluded that the elution peak resulting from a strong affinity chromatography is predictable using Eq. (23) provided that the non-retained fraction is sufficiently small.

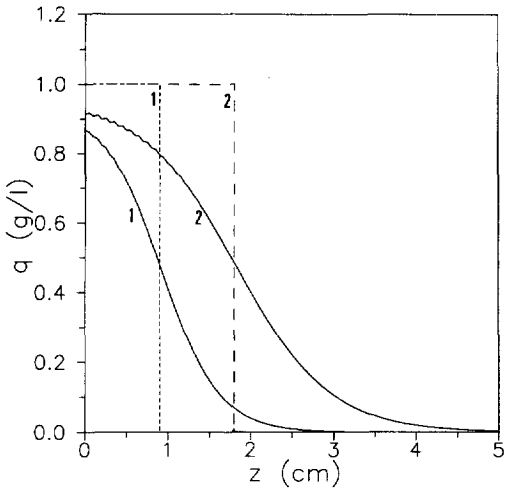

Fig. 16. Distributions of the adsorbate concentration at the starting time of the elution stage as functions of the axial distance along the column for strong affinity systems with $K_d = 2.15 \times 10^{-9}$ M and different adsorption rate constant, k_a (l g^{-1} s^{-1}), at the adsorption stage: (1) 0.75; (2) 0.45. The approximated profiles under the assumption of irreversible adsorption corresponding to the simulated systems are presented in dashed curves.

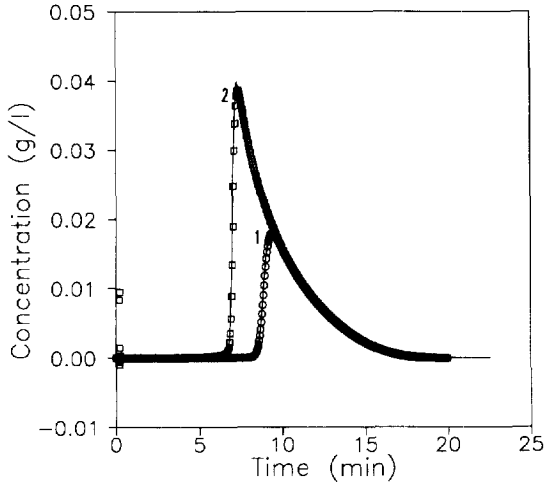

Fig. 17. Comparison of elution profiles from model simulation (data points) and the approximated elution profiles (solid curves) calculated by Eq. (23).

5. Conclusion

A model describing the peak behaviour of pH elution in high-performance affinity chromatography using non-porous adsorbents was solved numerically with the application of the finite element method. At a limiting case (isocratic elution), the numerical solutions approach the Goldstein solutions. The model simulation generates performance information of the elution needed to design an analytical chromatographic process, such as the non-retained fraction, the peak profile and the retention time under various operating conditions. The simulated results show the following.

Contributions of the adsorption rate constant (k_a) and equilibrium dissociation constants (K_d) under adsorption conditions are mainly to the split-peak effect. The non-retained fraction increases with the decrease of k_a and/or K_d. In addition to the effects of k_a and K_d under elution conditions, the elution peak also is influenced by these constants under the adsorption conditions. The latter influences are inherited from

the adsorbate profile along the column length at the beginning of the elution, i.e. the time when the mobile phase changes from the adsorption to the elution stages. In general, slow adsorption kinetics (small k_a) is shown to have a significant dispersive effect on the elution peak. When the rate constant under either adsorption or elution conditions becomes larger, the elution peak becomes sharper and the time required to elute all bound solutes becomes shorter due to the faster rate.

Besides being governed by k_a and K_d under adsorption conditions, the non-retained fraction is dominated by the sample loading. The split-peak effect becomes more significant whenever the binding capacity is relatively small compared to the sample load. In a limiting case of irreversible adsorption, simulation of the model yields the non-retained fraction which is in agreement with that predicted by an equation in the literature.

The mean retention time of the elution peak is dominated by the equilibrium dissociation constant under elution conditions. Alteration of the pH of the mobile phase is the most common way to increase the K_d value in order to shorten the elution time. If K_d cannot be greatly increased due to the strong elution conditions which are usually harmful and cause damage to the ligand, a lower ligand density (i.e. a small binding capacity) could be considered as an alternative.

The model simulation predicts the effect of sample load (sample concentration) on the performance of the elution peak, which provides an excellent basis for choosing a proper plot as a calibration graph. The straight line can easily be obtained from the plots of plate height vs. sample load for larger values of K_d. When the non-retained fraction is small, the elution peak resulting from pH elution of a strong affinity chromatography is predictable by the model simulation as well as a close-form expression describing the elution followed an irreversible adsorption.

6. Nomenclature

A_c cross-sectional area of the column, cm^2
c concentration of solute in mobile phase, $g\ l^{-1}$
c_s concentration of solute in the liquid at the surface of the adsorbent, $g\ l^{-1}$
c_0 sample concentration, $g\ l^{-1}$
D_L axial dispersion coefficient of solute, $cm^2\ s^{-1}$
D_m molecular diffusivity of solute, $cm^2\ s^{-1}$
d_p diameter of adsorbent particle, cm
g_i i-th quadratic basis function in every finite elements
k_0' capacity factor at zero sample concentration
K_a equilibrium association constant, M^{-1}
K_d equilibrium dissociation constant, M
k_a adsorption rate constant at adsorption or elution stage, $l\ g^{-1}s^{-1}$ or $M^{-1}s^{-1}$
k_d desorption rate constant at adsorption or elution stage, s^{-1}
k_f film mass transfer coefficient, $cm\ s^{-1}$
L length of the column, cm
n number of nodes
N non-dimensional parameter, $=(1-\epsilon)k_a q_m L/u_0$
N_e number of finite element
Pe Peclet number
Q_i amount of solute injected to the column, g
Q_s saturation binding capacity of the column, g
q adsorbate concentration, $g\ l^{-1}$
q_m maximum adsorbate concentration, $g\ l^{-1}$
t time, s
t_e time of elution starting, s
t_{inj} time interval of sample injection, s
t_R mean retention time of the elution peak, s
u_0 superficial velocity, $cm\ s^{-1}$
Z non-dimensional axial coordinate
z axial coordinate along the column, cm
z_0 length of the column saturated with adsorbate, cm

Greek letters

ϵ void fraction of the packed column
τ non-dimensional time
ν dynamic viscosity, $cm^2\ s^{-1}$

Superscripts

$*$ non-dimensional variables

Acknowledgements

This study was supported in part by the National Science Council of the Republic of China under contract NSC 84-2214-E194-006.

References

[1] Brian III, B.F., Zwiebel, I., Artigue, R.S. (1987), AIChE Symp. Ser., (Vol. 83), 80.
[2] Raghavan, N.S., Ruthven, D.M. (1983), AIChE J., (Vol. 29), 922.
[3] Arve, B.H., Liapis, A.I. (1987), Biotechnol. Bioeng., (Vol. 30), 638.
[4] Ma, Z., Guiochon, G. (1991), Comput. Chem. Eng., (Vol. 15), 415.
[5] Nguyen, T.S., Hu, S.-G., Do, D.D. (1992), Chem. Eng. J., (Vol. 49), B41.
[6] Whitley, R.D., Van Cott, K.E., Berninger, J.A., Wang, N.-H.L. (1991), AIChE J., (Vol. 37), 555.
[7] Gu, T., Tsai, G.-J., Tsai, G.T. (1990), AIChE J., (Vol. 36), 784.
[8] Hossain, M.M., Do, D.D. (1992), Chem. Eng. J., (Vol. 49), B29.
[9] Mao, Q.M., Johnston, A., Prince, I.G., Hearn, M.T.W. (1991), J. Chromatogr., (Vol. 548), 147.
[10] Anspach, B., Unger, K.K., Davies, J., Hearn, M.T.W. (1988), J. Chromatogr., (Vol. 475), 195.
[11] Liapis, A.I., Anspach, B., Findley, M.E., Davies, J., Hearn, M.T.W., Unger, K.K. (1989), Biotechnol. Bioeng., (Vol. 34), 467.
[12] Anspach, F.B., Johnston, A., Wirth, H.J., Unger, K.K., Hearn, M.T.W. (1990), J. Chromatogr., (Vol. 499), 103.
[13] Wirth, H.J., Unger, K.K., Hearn, M.T.W. (1990), J. Chromatogr., (Vol. 550), 383.
[14] Wongyai, S., Varga, J.M., Bonn, G.K. (1991), J. Chromatogr., (Vol. 536), 155.
[15] Tuncel, A., Denizli, A., Purvis, D., Lowe, C.R., Piskin, E. (1993), J. Chromatogr., (Vol. 634), 161.

[16] Hage, D.S., Walters, R.R., Hethcote, H.W. (1986), Anal. Chem., (Vol. 58), 274.
[17] Hage, D.S., Walters, R.R. (1988), J. Chromatogr., (Vol. 436), 111.
[18] Jaulmes, A., Vidal-Madjar, C. (1991), Anal. Chem., (Vol. 63), 1165.
[19] Place, H., Sebille, B., Vidal-Madjar, C. (1991), Anal. Chem., (Vol. 63), 1222.
[20] Renard, J., Vidal-Madjar, C. (1994), J. Chromatogr. A, (Vol. 661), 35.
[21] Lee, W.-C., Chuang, C.-Y. (1996), J. Chromatogr. A., (Vol. 721), 31.
[22] Chung, S.F., Wen, C.Y. (1968), AIChE J., (Vol. 14), 857.
[23] Wilson, E.J., Geankoplis, C.J. (1966), Ind. Eng. Chem. Fundam., (Vol. 5) (1), 9.
[24] Goldstein, S. (1953), Proc. Roy. Soc. Ser. A, (Vol. 219), 151.
[25] B.A. Finlayson, Nonlinear Analysis in Chemical Engineering, McGraw-Hill, New York, 1980, pp. 126.
[26] L. Lipidus, G.F. Pinder, Numerical Solution of Partial Differential Equations in Science and Engineering, Wiley, New York, 1982, pp. 286.
[27] Antonsen, K.P., Colton, C.K., Yarmush, M.L. (1991), Biotechnol. Progr., (Vol. 7), 159.
[28] Kang, K.A., Ryu, D.D. (1991), Biotechnol. Progr., (Vol. 7), 205.